Journal of Applied Polymer Science

Thermotropic Glazings for Overheating Protection. II. Morphology and Structure–Property Relationships

Andreas Weber,[1] Andrea Schmid,[2] Katharina Resch[2]

[1]Polymer Competence Center Leoben GmbH, Roseggerstrasse 12, 8700 Leoben, Austria

[2]Materials Science and Testing of Polymers, Department Polymer Engineering and Science, University of Leoben, Otto Glöckel-Strasse 2, 8700 Leoben, Austria

Correspondence to: K. Resch (E - mail: katharina.resch@unileoben.ac.at)

ABSTRACT: This article completes a systematic strategy for formulation and optimization of thermotropic systems with fixed domains (TSFDs) for overheating protection purposes. Focus was on characterization of morphology and on revealing optimization potential. A comprehensive characterization of scattering domain size and shape was done applying optical microscopy and scanning electron microscopy. In general, scattering domains exhibited inappropriate size and/or shape for optimum overheating protection performance. Moreover, several TSFD displayed defects (vacuoles, voids) resulting from thermomechanical or physicochemical interaction of matrix material and thermotropic additive during manufacturing. Morphological features along with solar optical and thermorefractive properties allowed for establishment of structure–property relationships. Light-shielding efficiency of TSFD correlated well with scattering domain size and shape. The majority of TSFD showing defects exhibited an increase of solar hemispheric transmittance upon heating. Several strategies to overcome defect formation and to improve scattering morphology were suggested and proof of concept was shown partially, thus indicating a significant optimization potential of the established TSFD. © 2013 Wiley Periodicals, Inc. J. Appl. Polym. Sci. **2014**, *131*, 39910.

KEYWORDS: structure–property relations; morphology; optical and photovoltaic applications; optical properties; photochemistry

Received 10 July 2013; accepted 29 August 2013

DOI: 10.1002/app.39910

INTRODUCTION

A feasible way to prevent buildings and solar thermal collectors from overheating are thermotropic glazings.[1–3] Thermotropic glazings change their light transmittance from highly transmitting to highly reflecting upon reaching a certain threshold temperature reversibly.[3–5] Besides other classes of thermotropic glazings, thermotropic systems with fixed domains (TSFD) gained interest in recent research due to their specific advantages like high reversibility, low hysteresis, ease of adjustment of switching threshold, high long-term stability, and their steep switching process.[6–17] TSFD consist of a thermotropic additive finely dispersed in a matrix material.[3,4] Refractive index difference of matrix and additive and TSFD morphology are of paramount importance for scattering performance and thus overheating protection performance of TSFD.[18] Refractive indices of matrix and additive are almost equal below the phase transition temperature (e.g., melting temperature) of the additive yielding transparent appearance of the TSFD.[4] Upon exceeding the switching threshold the refractive index difference between matrix and additive increases steeply resulting in a reduction of solar hemispheric transmittance.[4] Maximum light-shielding efficiency is attained by spherical scattering domains with diameters in the range between 200 and 400 nm.[18]

So far with TSFD only moderate overheating protection performance was achieved. Limited light-shielding performance was primarily ascribed to inappropriate scattering domain size and shape.[6–10,12,16] Thus, Weber and Resch[17] carried out a systematic and comprehensive evaluation of numerous TSFD based on a novel material formulation and characterization strategy to evaluate overheating protection and optimization potential. Candidate matrix materials and thermotropic additives were characterized comprehensively based on sound polymer-physical principles. Promising material combinations were formulated. On the one hand side, TSFDs exhibiting the aspired decrease in solar hemispheric transmittance upon exceeding the threshold temperature were achieved. On the other hand side, TSFDs displaying an increase in solar hemispheric transmittance were attained. Hence, the major objective of this article is to establish relationships between observed switching characteristics and TSFD specific material properties (thermorefractive properties of matrix and additive, morphology, etc.). For this purpose, a comprehensive characterization of TSFD morphology is carried

out. Subsequently, material optimization approaches are derived to improve overheating protection performance.

SYSTEMATIC MATERIAL FORMULATION STRATEGY

Refractive index difference of matrix and additive and TSFD morphology are of paramount importance for scattering performance and thus overheating protection performance of TSFD.[18] Hence, for the development of novel TSFD a systematic material formulation strategy has been established to account for these factors. The strategy comprises seven different steps. First, a comprehensive literature review concerning material properties is carried out to evaluate candidate matrix materials and thermotropic additives: Matrix materials exhibit preferably high transition temperatures (glass transition, melting), high transmittance and a refractive index as low as possible. Thermotropic additives must display a thermal transition—preferably melting—between 30°C and 105°C along with a rapid and steep change of refractive index. Subsequently, a comprehensive polymer-physical characterization of candidate matrix materials and thermotropic additives with regard to thermal, thermomechanical and optical properties is carried out. In the second step, appropriate combinations of candidate matrix materials and thermotropic additives are identified by assessment of refractive index match/mismatch. Based on this evaluation procedure promising TSFD are formulated and characterized as to light-shielding efficiency, switching characteristics and threshold temperature. Finally, a comprehensive characterization of morphology (scattering domain size, shape, distribution) is carried out and structure–property relationships are established. Based on these interrelationships optimization potential of TSFD is deduced. These final steps are addressed within the present article. The preceding steps are already covered in a previous publication.[17]

CHARACTERIZATION OF MORPHOLOGY

Experimental

Materials and Sample Preparation. Three thermoplastic matrix materials (M1 to M3), four UV-curable resin systems (M4 to M7) and 13 different thermotropic additives (A1 to A11, A20, and A21) were utilized for formulation of TSFD. A detailed description of matrix materials and thermotropic additives is given in the preceding publication.[17] TSFD with thermoplastic matrix were manufactured at APC Advanced Polymer Compounds (Gai, AT) by melt blending on a compounder Coperion ZSK 26 Mcc (Coperion GmbH, Stuttgart, DE). From the compound 800 μm thick plates were obtained by compression molding on a press P200PV (Dr. Collin GmbH, Ebersberg, DE). Thermotropic layers based on UV-curable resin matrix were prepared by dissolving the thermotropic additive in the UV-crosslinkable matrix solution, which consisted of 57 wt % oligomers, 40 wt % reactive diluent, and 3 wt % photoinitiator.[17] The dissolutions were poured in the intervening space between two glass panes which were sealed around the edge and stored at ambient temperature for 10 min allowing for precipitation of the additive. Afterwards the mixtures were cured by UV-radiation (dose: 2.1 J cm^{-2}) from a Light Hammer 6 equipped with a mercury-lamp and a LC6E Benchtop Conveyor (Fusion UV Systems Inc., Gaithersburg, MD). Free standing layers with a thickness of 900 μm were obtained after removal of the glass panes. TSFD based on UV-curable resin matrix were annealed at the mixing temperature of matrix solution and the corresponding additive. For both, thermoplastic and resin based TSFD, the theoretical additive concentration was 5 wt %. As to nomenclature, a system composed of Matrix M1 and Additive A1 is named M1A1.[17]

Characterization Methodology. Morphological characterization of TSFD was carried out applying optical light microscopy (LiMi) and scanning electron microscopy (SEM). Optical micrographs were obtained with an optical microscope Olympus BX51 (Olympus Austria Ges. m. b. H., Wien, AT) in transmitted light mode from TSFD without further preparation. Samples intended for SEM were cut with a knife to achieve a fragment of ~14 mm × 5 mm × 0.9 mm. Fragment was fixed with a Plastic Specimen Support Clip (Buehler, Lake Bluff, IL), inserted in a beaker and embedded in a mixture of EpoThin Epoxy Resin and EpoThin Epoxy Hardener (Buehler). After hardening, specimens were ground successively with different abrasive disks (P 600, P 1200, P 2400, P 4000) applying a force of 15 N under constant water flow in counter-rotating mode (200 rpm) on a grinder/polisher Phoenix Beta (Buehler). Subsequently specimens were polished with MetaDi Monocrystalline Diamond Suspension on Polishing Cloth and with lubricant MetaDi Fluid, Dialub SW (Buehler). Specimens were rinsed thoroughly with water between the individual grinding/polishing steps. Prior to imaging with SEM DSM 962 (Carl Zeiss SMT AG, Oberkochen, DE), the specimens were sputtered with gold.

Domain size was evaluated with measurement tools of software analySIS (Soft Imaging System GmbH, Münster, DE). Minimum and maximum of individual scattering domain dimensions were evaluated. Multiple determinations were carried out on a representative specimen for each TSFD. An increased number of specimens (up to three) were investigated for TSFD with inconsistent (i.e., divergence) switching behavior detected by UV/Vis/NIR spectrophotometry.

Results

Figure 1 depicts the four prevalent scattering domain types detected for TSFD investigated within this study. SEM images are shown only due inappropriate contrast of optical micrographs for printing. Several TSFD exhibited spherical scattering domains. Additionally, some of these TSFD displayed significant gaps at the circumference (vacuoles) of the spherical scattering domains [Figure 1(a,b)]. However, most of these vacuoles appeared rather like a dent in the additive domain than like a shell around the additive particle. Other TSFD showed scattering domains resembling plate-like features [Figure 1(c,d)]. Furthermore, scattering domains resembling balls of filaments, thus named filament spheres, with a significant number of voids between the individual filaments were observed [Figure 1(e,f)]. Other TSFD displayed structures characterized by individual branches originating from a central node and successive subbranches, thus named dendrites [Figure 1(g,h)].

Tables I and II summarize morphological features detected by optical light microscopy (LiMi) and SEM of different TSFD. If

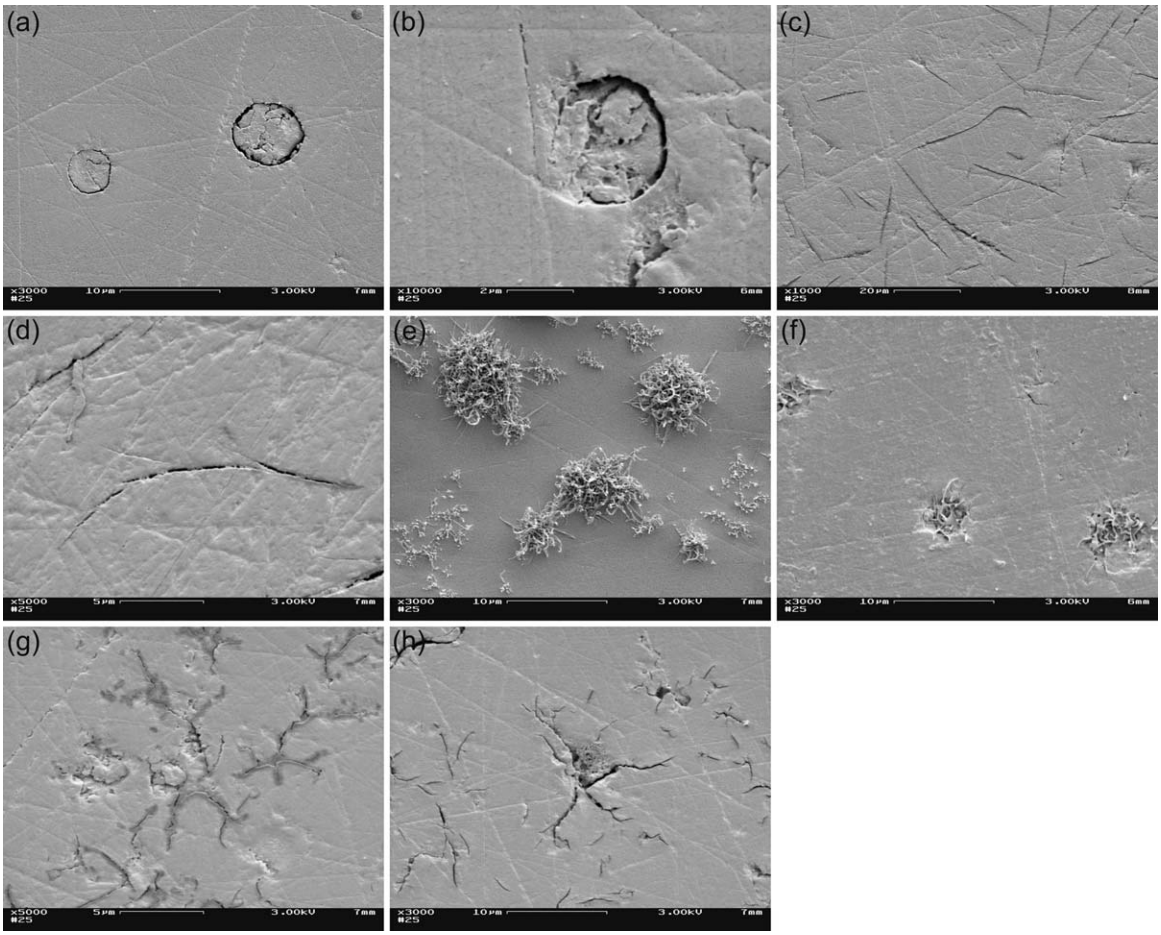

Figure 1. Representative SEM micrographs of scattering domain shapes distinguished within this study: Spherical domains, with vacuoles from TSFD (a) M7A1 and (b) M5A2; plate-like domains from TSFD (c) M6A3 and (d) M4A3; filament spheres from TSFD (e) M5A7 and (f) M7A4; and dendrites from TSFD (g) M4A8 and (h) M7A8.

domains were detectable, their shape and size are stated, otherwise cells are left blank. Cells are partially left blank if one parameter was not detected by LiMi but by SEM or vice versa. Size parameters are divided in two dimensions to be able to handle nonspherical domains also. Dimension L_1 represents the major dimension of the scattering domain (e.g., diameter) whereas dimension L_2 is only valid for nonspherical scattering domains representing the minor dimension (e.g., thickness). Detected defects (e.g., vacuoles) are listed in a separate column. Table I summarizes morphological features for TSFD with thermoplastic matrix material. TSFD M1A1, M1A2, M1A11, M2A2, M2A6, M2A11, M3A20, and M3A21 exhibited spherical

Table I. Shape of Scattering Domains, Minima and Maxima of Dimensions L_1 (Major Dimension) and L_2 (Minor Dimension, If Applicable) and Detected Defects of TSFD Formulated with Thermoplastic Matrix Materials

Material	Shape of domains	Dim. L_1 (min.) (μm) LiMi/SEM	Dim. L_1 (max.) (μm) LiMi/SEM	Dim. L_2 (min.) (μm) LiMi/SEM	Dim. L_2 (max.) (μm) LiMi/SEM	Defects
M1A1	Spheres	0.39/1.06	12.1/67.3	na/na	na/na	Vacuoles
M1A2	Spheres	0.41/3.25	13.3/32.3	na/na	na/na	Vacuoles
M1A11	Spheres	0.50/6.62	7.64/123	na/na	na/na	Vacuoles
M2A2	Spheres	0.44/1.90	30.8/13.5	na/na	na/na	Vacuoles
M2A6	Spheres	0.39/–	8.88/–	na/na	na/na	Vacuoles
M2A11	Spheres	0.59/–	5.30/–	na/na	na/na	
M3A20	Spheres	0.50/–	9.97/–	na/na	na/na	
M3A21	Spheres	0.31/–	8.85/–	na/na	na/na	

na: not applicable; –: not evaluable/not detectable.

Table II. Shape of Scattering Domains, Minima and Maxima of Dimensions L_1 (Major Dimension) and L_2 (Minor Dimension, If Applicable) and Detected Defects of TSFD Formulated with UV-Curable Resin Matrix

Material	Shape of domains	Dim. L_1 (min.) (μm) LiMi/SEM	Dim. L_1 (max.) (μm) LiMi/SEM	Dim. L_2 (min.) (μm) LiMi/SEM	Dim. L_2 (max.) (μm) LiMi/SEM	Defects
M4A1	Spheres	0.84/2.55	194/235	na/na	na/na	Vacuoles
M4A2	Spheres	0.78/0.87	67.9/143	na/na	na/na	Vacuoles
M4A3	Plates	6.77/3.24	50.0/54.2	0.20/0.16	1.79/0.57	
M4A5	Dendrites	0.50/4.69	39.3/22.7	0.39/0.81	0.98/4.50	
M4A6	Spheres	0.50/1.04	65.8/32.1	na/na	na/na	Vacuoles
M4A7	Dendrites	13.7/7.38	48.9/23.5	0.44/1.01	1.27/3.92	
M4A8	Dendrites	-/3.47	-/15.2	-/0.08	-/0.35	
	Spheres	-/1.47	-/8.34	na/na	na/na	
M4A9	Spheres	6.47/-	158/-	na/na	na/na	Vacuoles
M4A10	Dendrites	13.3/13.1	28.9/30.7	0.50/1.1	1.79/2.72	
M5A1	Spheres	1.49/1.04	64.6/43.6	na/na	na/na	Vacuoles
M5A2	Spheres	1.71/2.04	55.2/22.3	na/na	na/na	Vacuoles
M5A3	Plates	8.04/7.02	65.3/75.5	0.20/0.25	2.75/1.91	Cracks
M5A4	Filament spheres[a]	4.85/2.93	54.5/56.1	-/0.18	-/0.55	Voids
M5A5	Dendrites	6.62/6.50	22.7/23.4	0.44/0.48	0.84/2.42	
M5A6	Spheres	0.74/1.40	52.2/31.2	na/na	na/na	Vacuoles
M5A7	Filament spheres[a]	0.59/3.97	17.6/23.9	-/0.07	-/3.37	Voids
M5A8	Dendrites	1.38/3.53	24.1/12.1	-/0.18	-/0.89	
M5A9	Spheres	7.41/12.2	40.5/45.6	na/na	na/na	
M5A10	Dendrites	7.95/5.45	17.0/16.1	0.39/0.71	1.00/1.74	
M6A1	Spheres	0.87/2.49	5.02/139	na/na	na/na	Vacuoles
M6A2	Spheres	2.07/1.88	7.95/3.83	na/na	na/na	Vacuoles
M6A3	Plates	6.47/4.06	52.1/44.0	0.62/0.11	2.23/1.12	
M6A10	Dendrites	9.66/9.52	20.9/25.3	0.59/0.88	1.85/5.74	
M7A1	Spheres	3.87/1.88	60.3/59.6	na/na	na/na	Vacuoles
M7A2	Spheres	0.93/0.93	58.0/2.92	na/na	na/na	Vacuoles
M7A3	Plates	10.8/6.26	69.1/46.0	0.59/0.17	2.48/1.59	
M7A4	Filament spheres[a]	2.07/13.8	133/94.4	-/0.17	-/1.08	Voids
M7A5	Dendrites	13.1/5.7	24.2/23.0	0.93/0.88	2.99/3.75	
M7A6	Spheres	0.59/8.19	42.3/40.3	na/na	na/na	
M7A7	Filament spheres[a]	7.18/1.22	50.5/37.6	0.39/0.05	1.31/0.30	Voids
M7A8	Dendrites	-/3.49	-/22.5	-/0.16	-/0.70	
M7A9	Spheres	13.3/12.1	45.0/62.2	na/na	na/na	
M7A10	Dendrites	15.2/3.48	28.7/29.6	1.17/0.58	2.34/2.55	

[a] Spheres built up from filaments.
na: not applicable; -: not evaluable/not detectable.

scattering domains with diameters ranging between 0.31 and 123 μm. Moreover, micrographs revealed existence of vacuoles for layers M1A1, M1A2, M1A11, M2A2, and M2A6. For several TSFD, the scattering domain sizes detected by LiMi and SEM differ significantly. On the one hand side, that may be attributed to higher accuracy of measurements in SEM images compared to optical light micrographs due to higher achievable magnification and thus higher resolution. This is especially relevant for small features. On the other hand side, that can be an indication for low uniformity of the layers. Certain regions in a TSFD might exhibit a higher concentration of specifically sized scattering domains than other regions.

Table II summarizes morphological features of TSFD with UV-curable resin matrix. TSFD M4A1, M4A2, M4A6, M4A8, M4A9, M5A1, M5A2, M5A6, M5A9, M6A1, M6A2, M7A1, M7A2, M7A6, and M7A9 displayed spherical scattering domains with diameters in the range between 0.50 and 235 μm. Micrographs revealed existence of vacuoles for layers M4A1, M4A2, M4A6, M4A9, M5A1, M5A2, M5A6, M6A1, M6A2, M7A1, and M7A2. However, in M4A9 only one out of three samples displayed a

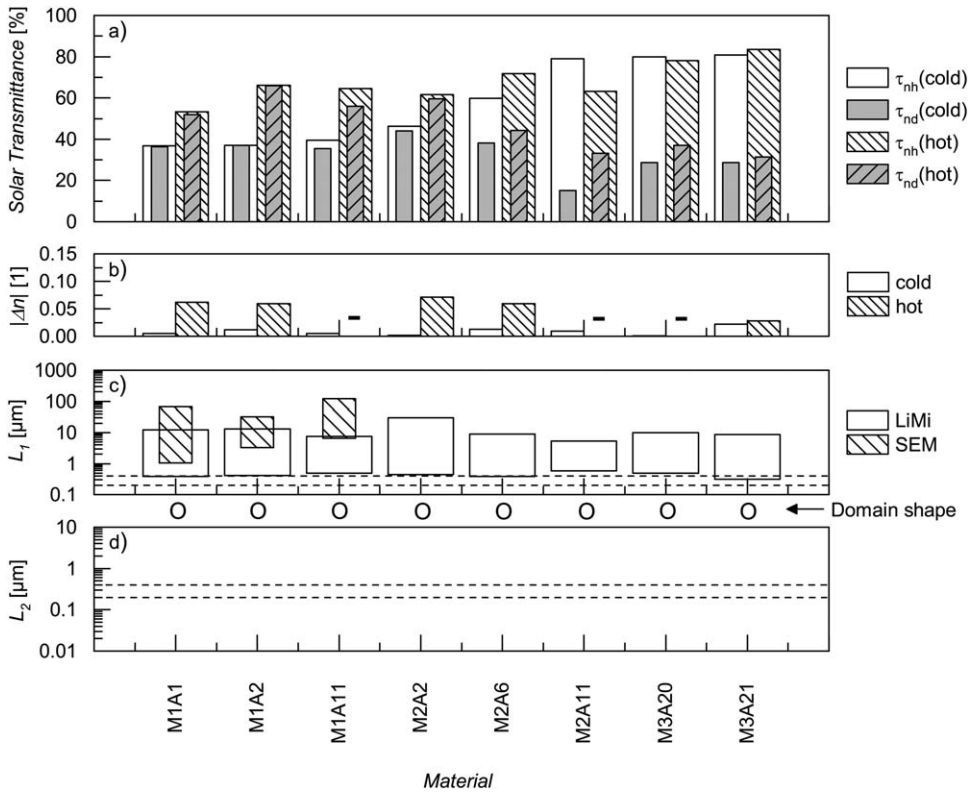

Figure 2. (a) Solar hemispheric (τ_{nh}; base color white) and solar diffuse transmittance (τ_{nd}; base color gray) of TSFD formulated with thermoplastic matrix material below (no pattern) and above (hatching pattern) the threshold temperature (data from Part I[17]). (b) Refractive index difference of matrix and additive below (no pattern) and above (hatching pattern) the threshold temperature. Omitted values are indicated by "-". Observed scattering domain shapes indicated with symbols ("O" spheres) and their respective dimensions (c) L_1 (diameter) and (d) L_2 (if applicable, thickness of plates/filaments/dendrite branches) detected by optical light microscopy (LiMi; no pattern) and SEM (hatching pattern). Optimum scattering domain size range for spherical scattering domains is bounded by dashed lines.

significant number of vacuoles. Layers M4A3, M5A3, M6A3, and M7A3 exhibited plate-like scattering domains with diameters and thicknesses ranging from 3.24 to 75.5 µm and from 0.11 to 2.75 µm, respectively. In TSFD M5A3 persistent cracks were formed upon heating. TSFD M5A4, M5A7, M7A4, and M7A7 showed scattering domains resembling filament spheres with diameters between 0.59 and 133 µm and voids between the filaments. Thickness of the single filaments varied between 0.05 and 3.37 µm. Layers M4A5, M4A7, M4A8, M4A10, M5A5, M5A8, M5A10, M6A10, M7A5, M7A8, and M7A10 displayed dendritic scattering domains with diameters and thicknesses of branches varying from 0.5 to 48.9 µm and between 0.08 and 5.74 µm, respectively. Interestingly, for TSFD M4A8 two different scattering domain shapes—spheres and dendrites—were distinguished. None of the TSFD investigated exhibited optimal scattering domain shape and size for efficient overheating protection performance.[18] For several TSFD, the scattering domain sizes detected by LiMi and SEM differ significantly. On the one hand side, that may be attributed to higher accuracy of measurements in SEM images compared to optical light micrographs due to higher achievable magnification and thus higher resolution. This is especially relevant for small features. On the other hand side, that can be an indication for low uniformity of the layers. Certain regions in a TSFD might exhibit a higher concentration of specifically sized scattering domains than other regions.

ESTABLISHMENT OF STRUCTURE-PROPERTY RELATIONSHIPS

In Figures 2–6, average solar hemispheric (τ_{nh}; base color white) and diffuse transmittance (τ_{nd}; base color gray) investigated within this study are depicted for a temperature below (no pattern) and above (hatching pattern) the threshold temperature, respectively [Figures 2(a)–6(a)]. Data originate from Part I of this publication series.[17] Absolute refractive index difference of matrix material and thermotropic additive below (white column) and above the threshold temperature (hatched column) are also illustrated [Figures 2(b)–6(b)]. Unless otherwise is stated in general, for each of the TSFD discussed herein refractive index data theoretically indicate a reduction of solar hemispheric transmittance above the switching threshold.[17] Furthermore, in Figures 2–6, observed domain shape is indicated by symbols ("O" spheres; "/" plates; "Θ" filament spheres; "*" dendrites). The dimensions L_1 [diameter: O, /, Θ, *; Figures 2(c)–6(c)] and L_2 [thickness of plate/filament/dendrite branch: / , Θ, *; Figures 2(d)–6(d)] of these domains are represented by floating columns. Size ranges of scattering domains detected by optical microscopy (no pattern) and SEM (hatching pattern) are displayed separately. Optimum diameter range of spherical scattering domains is bounded by dashed lines. For clarity

reasons, in the following layers displaying the same domain shape are grouped for discussion: Structure–property relationships of TSFD exhibiting scattering domains with appropriate shape for optimum light-shielding efficiency (spherical) are discussed in the first place for each figure. Subsequently, structure–property relationships of TSFD displaying scattering domains with inappropriate shape for efficient overheating protection performance (plate-like domains, filament spheres, dendrites) are discussed.

Figure 2 represents parameters indicated above for TSFD with thermoplastic matrix material. For these TSFD merely spherical scattering domains ("O") were observed. Spherical scattering domains of TSFD M1A1, M1A2, M1A11, M2A2, and M2A6 exhibited diameters hardly in the optimum range between 200 and 400 nm for efficient light-shielding performance and vacuoles at their perimeter (interface matrix/additive). Vacuole formation may be attributed to different coefficient of thermal expansion (CTE) of matrix material and additive. The CTE of PMMA and paraffin for example are in the range of 6–8 $\times$ 10^{-5} and 0.7–1.1 $\times$ 10^{-3} K^{-1}, respectively.[19,20] The higher CTE of paraffin forced the embedded additive to contract more intense than the surrounding matrix PMMA upon cooling during manufacturing, thus yielding formation of vacuoles when implying limited adhesion at the interface matrix/additive.[17,21,22] All of these layers displayed an increase in solar hemispheric and diffuse transmittance upon heating.

Morphological investigations now confirm assumptions concerning relations between increase in solar hemispheric transmittance and the presence of vacuoles.[17] Dimensions of dent-like vacuoles were theoretically equal (maximum) to or smaller than the size of the cavity provided by the matrix. Accordingly the rest of the cavity was filled with additive. Shell-like vacuoles theoretically had the same diameter as their respective matrix cavities but were larger than the corresponding additive domain inside the cavity. However, thickness of the shell-like vacuoles was low compared to diameter. Thus, a virtual (envisaged) vacuole size distribution probably showed a significantly lower minimum and mean and a slightly higher maximum compared to the additive domain size distribution. Virtually merging these two size distributions in a thought experiment yielded a broad "virtual" size distribution of scattering domains. The high difference in refractive index of matrix material ($n \sim 1.5$) and vacuole ($n = 1$) along with smaller size of vacuoles compared to additive domains resulted in intense scattering and hence low solar hemispheric transmittance at room temperature.[17] On the contrary, the refractive index difference of matrix and additive below the switching threshold was negligible. Thus, effect of additive domains on forward scattering intensity was low, yielding low solar diffuse transmittance. Upon heating and especially upon melting the additive expanded and filled the cavity completely, yielding a decrease in refractive index difference at the scattering interface. Moreover, the virtual size distribution narrowed upon disappearance of the vacuoles and thus was identical with the actual size distribution of the additive domains. Thus, mean value of scattering domain size was also shifted to higher values. In general, solar hemispheric transmittance gained from a decrease in refractive index difference due to a reduction of overall scattering performance. An isolated increase in scattering domain size increased anisotropy of scattering field yielding reduced back-scattering and increased forward-scattering efficiency. Accordingly, a simultaneous reduction of refractive index difference along with an increase in scattering domain size reduced the overall scattering performance of the TSFD and made the scattering field more anisotropic. Thus solar hemispheric transmittance increased upon heating. An increase in scattering field anisotropy did not necessarily yield an increase in solar diffuse transmittance. Especially for non-spherical scattering domain effects of geometry and potential domain internal boundaries (e.g., voids inside the additive domain) might be rather complex, either yielding an increase or a decrease in solar diffuse transmittance. However, the effect of vacuoles on switching characteristics of TSFD is going to be addressed as "*effect of the temporary vacuoles*" within this study.

In contrast, for layers displaying spherical scattering domains with inappropriate size for efficient light-shielding performance but lacking vacuoles a rather moderate reduction of solar hemispheric transmittance was expected upon heating. Simultaneously an increase in solar diffuse transmittance was anticipated. Nevertheless, this required a sufficient increase in refractive index difference between matrix and additive to be established upon heating. A prominent example for consistency of these predictions is TSFD M2A11, which showed spherical scattering domains with inappropriate diameter. Thus, the layer exhibited merely a moderate reduction of solar hemispheric transmittance upon exceeding the threshold temperature, along with an increase in solar diffuse transmittance. Although refractive index difference above the threshold temperature (75°C[17]) is not stated due to experimental reasons (for details refer to Weber and Resch[17]), observed switching characteristics implied an increase of refractive index difference upon switching. The lack of vacuoles within this TSFD may be attributed to the capability of amide-groups of matrix M2 and epoxy-moieties of A11 to form covalent bonds. Spherical scattering domains with inappropriate size for efficient light-shielding performance were detected for layers M3A20 and M3A21. Only minor changes in solar hemispheric transmittance were obtained for these TSFD along with a slight increase in solar diffuse transmittance. Refractive index difference of layer M3A20 is not stated for temperatures above the switching temperature (80°C[17]) due to experimental reasons.[17] However, negligible reduction of solar hemispheric transmittance implied only minor changes in refractive index difference. Layer M3A21 displayed a smooth change in transmittance rather than distinct switching.[17] This was attributed to insufficient change in refractive index difference.

For layers based on thermoplastic resin matrix, the observation of solely spherical scattering domains for nonpolar thermotropic additives like paraffin waxes (A1, A2) on the one hand side as well as for rather polar additives with maleic anhydride moieties (A11) on the other hand side was detected. That leads to the conclusion that establishment of TSFD morphology for these systems was governed by system rheology: In emulsions, spheres or ellipsoids are the prevalent droplet shapes.[23]

Figure 3 represents parameters indicated above for TSFD with UV-curable matrix material M4. Observed domain shapes were

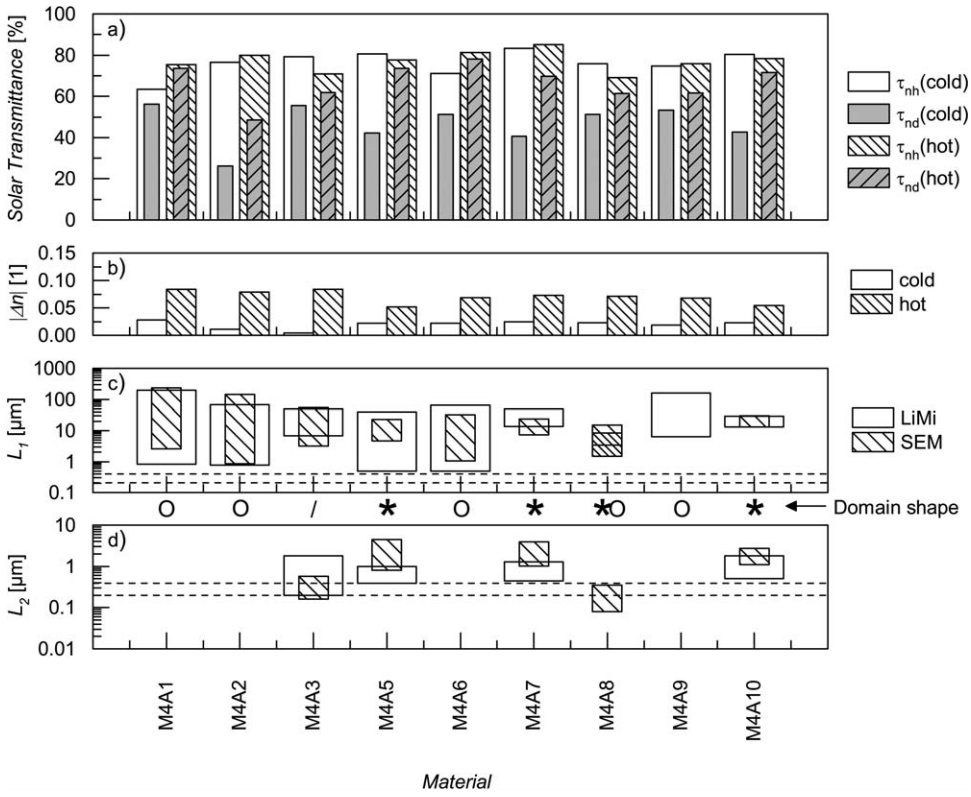

Figure 3. (a) Solar hemispheric (τ_{nh}; base color white) and solar diffuse transmittance (τ_{nd}; base color gray) of TSFD with UV-curable matrix material M4 below (no pattern) and above (hatching pattern) the threshold temperature (data from Part I[17]). (b) Refractive index difference of matrix and additive below (no pattern) and above (hatching pattern) the threshold temperature. Observed scattering domain shapes indicated with symbols ("O" spheres; "/" plates; "*" dendrites) and their respective dimensions (c) L_1 (diameter) and (d) L_2 (if applicable, thickness of plates/filaments/dendrite branches) detected by optical light microscopy (LiMi; no pattern) and SEM (hatching pattern). Optimum scattering domain size range for spherical scattering domains is bounded by dashed lines.

spheres ("O"), plate-like domains ("/") and dendrites ("*"). Spherical scattering domains with inappropriate diameter for efficient light-shielding performance and with vacuoles at their perimeter (interface matrix/additive) were detected for TSFD M4A1, M4A2, and M4A6. Vacuole formation was ascribed to processing effects[17]: mixtures of UV-curable resin and thermotropic additive were exposed to UV-radiation yielding crosslinking reaction in the matrix and heating up of the mixture due to absorption.[17] Upon cooling during manufacturing its higher CTE forced the embedded additive to contract more intensively than the surrounding matrix material, thus yielding formation of vacuoles when implying limited adhesion at the interface matrix/additive.[17,21,22] Layers M4A1, M4A2, and M4A6 displayed an increase in solar hemispheric and diffuse transmittance upon exceeding the threshold temperature. This was attributed to vacuoles rather than to inappropriate scattering domain size, as already described above.

Spherical scattering domains with inappropriate size for efficient light-shielding performance were detected for TSFD M4A9. Samples 1 and 2 of these TSFD displayed a negligible concentration of vacuoles. However, Sample 3 displayed a significant concentration of vacuoles. Samples 1, 2, and 3 displayed solar hemispheric transmittance of ~81% (Samples 1 and 2) and ~62% (Sample 3) at room temperature, respectively, resulting in high standard deviation of mean transmittance.[17] The foremost samples attained a decrease of solar hemispheric transmittance to ~76% upon heating, whereas solar hemispheric transmittance of the latter sample increased to ~75%. Low solar hemispheric transmittance at room temperature and its increase for Sample 3 were attributed to significant concentration of vacuoles. For Samples 1 and 2, the increase in solar diffuse transmittance upon heating was attributed to inappropriate size of scattering domains. Solar diffuse transmittance increase in Sample 3 was ascribed to the effect of temporary vacuoles. A specific reason for selective formation of a high number of vacuoles in Sample 3 was not identified, because all layers were produced simultaneously.

Plate-like domains with inappropriate diameter but almost optimum thickness for efficient light-shielding performance were detected for TSFD M4A3, yielding a moderate reduction of solar hemispheric transmittance and an increase in solar diffuse transmittance upon exceeding the threshold temperature. Dendritic scattering domains with inappropriate diameter and thickness of dendrite branches for efficient overheating protection performance were evident for layers M4A5, M4A7, and M4A10. Thus, solar hemispheric transmittance remained almost

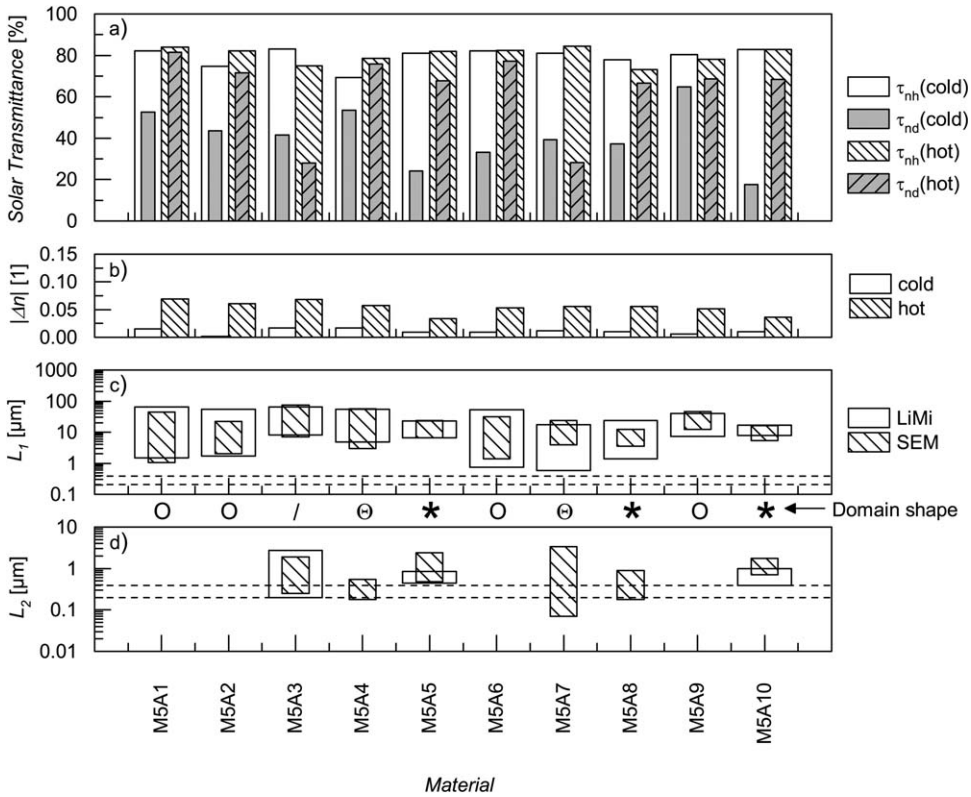

Figure 4. (a) Solar hemispheric (τ_{nh}; base color white) and solar diffuse transmittance (τ_{nd}; base color gray) of TSFD with UV-curable matrix material M5 below (no pattern) and above (hatching pattern) the threshold temperature (data from Part I[17]). (b) Refractive index difference of matrix and additive below (no pattern) and above (hatching pattern) the threshold temperature. Observed scattering domain shapes indicated with symbols ("O" spheres; "/" plates; "Θ" filament spheres; "*" dendrites) and their respective dimensions (c) L_1 (diameter) and (d) L_2 (if applicable, thickness of plates/filaments/dendrite branches) detected by optical light microscopy (LiMi; no pattern) and SEM (hatching pattern). Optimum scattering domain size range for spherical scattering domains is bounded by dashed lines.

unchanged (insignificant change[17]) upon heating whereas solar diffuse transmittance increased. TSFD M4A8 displayed scattering domains with spherical and dendritic shape, exhibiting inappropriate diameters for efficient light-shielding. However, thickness of dendrite branches was almost optimum for backscattering. Hence, a slight reduction of solar hemispheric transmittance was ascertained upon heating along with an increase in solar diffuse transmittance.

Figure 4 represents parameters indicated above for TSFD with UV-curable matrix material M5. Observed domain shapes were spheres ("O"), plate-like domains ("/"), filament spheres ("Θ") and dendrites ("*"). Spherical scattering domains with inappropriate size for optimum light-shielding and with vacuoles at their perimeter (interface matrix/additive) were detected for TSFD M5A1, M5A2, and M5A6. Layers M5A1 and M5A2 displayed an increase of solar hemispheric and diffuse transmittance upon heating due to effects resulting from vacuoles as already described above (effect of the temporary vacuoles). On the contrary solar hemispheric transmittance of layer M5A6 remained almost unchanged upon heating probably due to concentration effects (lower number of vacuoles yielded a vacuole effect of minor extent). Solar diffuse transmittance of TSFD M5A6 also increased upon heating. This was primarily attributed to inappropriate scattering domain size. TSFD M5A9 displayed spherical scattering domains with inappropriate diameter for efficient light-shielding performance, yielding a minor reduction in solar hemispheric transmittance along with an increase in solar diffuse transmittance upon heating.

Plate-like domains with inappropriate diameter but almost optimal thickness for efficient light-shielding performance were evident for TSFD M5A3. However, investigations revealed incoherent switching behavior of the three samples investigated.[17] One sample displayed a decrease of solar hemispheric transmittance upon heating along with an increase in solar diffuse transmittance. The onset of the observed decrease in solar hemispheric transmittance of Sample 1 at 55°C corresponds with the melting of the additive.[17] However, after cooling to room temperature, solar hemispheric and diffuse transmittance was lower and higher than in initial state (before heating), respectively. Maybe cracks (vacuum inside, refractive index 1) formed during measurement process acted as additional scattering domains,[17] thus increasing scattering volume. As a consequence low solar hemispheric transmittance and high solar diffuse transmittance was attained. In contrast, two other samples of layer M5A3 displayed a moderate increase of solar hemispheric transmittance upon heating along with a distinct reduction of solar diffuse transmittance. However, after cooling to room temperature, solar hemispheric and diffuse

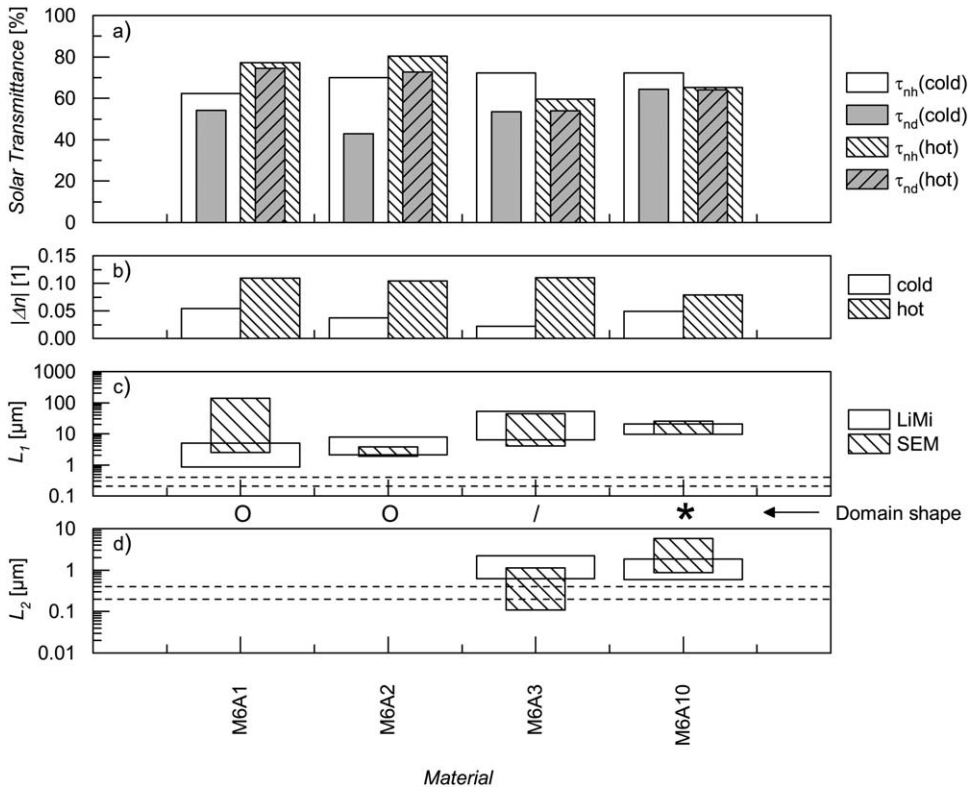

Figure 5. (a) Solar hemispheric (τ_{nh}; base color white) and solar diffuse transmittance (τ_{nd}; base color gray) of TSFD with UV-curable matrix material M6 below (no pattern) and above (hatching pattern) the threshold temperature (data from Part I[17]). (b) Refractive index difference of matrix and additive below (no pattern) and above (hatching pattern) the threshold temperature. Observed scattering domain shapes indicated with symbols ("O" spheres; "/" plates; "*" dendrites) and their respective dimensions (c) L_1 (diameter) and (d) L_2 (if applicable, thickness of plates/filaments/dendrite branches) detected by optical light microscopy (LiMi; no pattern) and SEM (hatching pattern). Optimum scattering domain size range for spherical scattering domains is bounded by dashed lines.

transmittance was lower and higher than in initial state (before heating), respectively, which was attributed to cracks as described above.

Regarding the crack formation process, only a hypothesis was established. Upon melting of the thermotropic additive, solar hemispheric transmittance of sample decreased due to melting and probably due to solubilization of additive molecules in the matrix. Due to concentration gradients of additive molecules, they started to diffuse inside the matrix. These molecules probably filled the free space close to the molecule chains of the matrix, yielding inability of these molecule chains to move unhindered (anti-plasticizer effect). The constraint of molecular movement probably yielded the inability to relax thermally induced stress upon increasing temperature, hence yielding crack formation. This corresponds with the continuous decrease in solar hemispheric transmittance of Sample 1 up to 115°C (increment 5°C). In contrast, solar transmittances of Samples 2 and 3 were detected at room temperature and 115°C only. Thus, time for migration of molten additive was very short, yielding less progress of crack formation process. This corresponds with the observation of small hazy areas evident in Samples 2 and 3, whereas Sample 1 displayed large hazy areas and distinct cracks.[17]

Micrographs of TSFD M5A4 and M5A7 revealed spherical scattering domains built from filaments. The diameters of these domains were inappropriate for optimum back-scattering. Thickness of the filaments was detected to be almost optimal for efficient light-shielding. However, between these filaments, voids were observed. Voids were assumed to act in the same manner as vacuoles. Thus, the ascertained increase of solar hemispheric transmittance of layers M5A4 and M5A7 was attributed to voids (effect of the temporary vacuoles/voids). Solar diffuse transmittance of TSFD M5A4 increased upon heating. In contrast, solar diffuse transmittance of M5A7 decreased upon switching. Divergence in change of solar diffuse transmittance of layers M5A4 and M5A7 is most likely due to effects of scattering domain geometry (e.g., slight differences in void concentration or distribution), yielding different scattering performance of the filament spheres. However, formation of voids seemed to be due to physicochemical interaction (nucleation, surface tension, etc.) of matrix material and thermotropic additive. If it was an additive related effect solely, layer M4A7 would have shown filament spheres also. Layers formulated with UV-curable matrix M4 contracted more upon exposure to UV-radiation compared to layers formulated with matrices M5, M6, and M7. Stronger contraction of the matrix likely introduced higher internal stress in the layer. Hence, high internal stress probably forced the additive to crystallize in filament sphere shape rather than in dendritic shape as in TSFD M5A7 and M7A7.

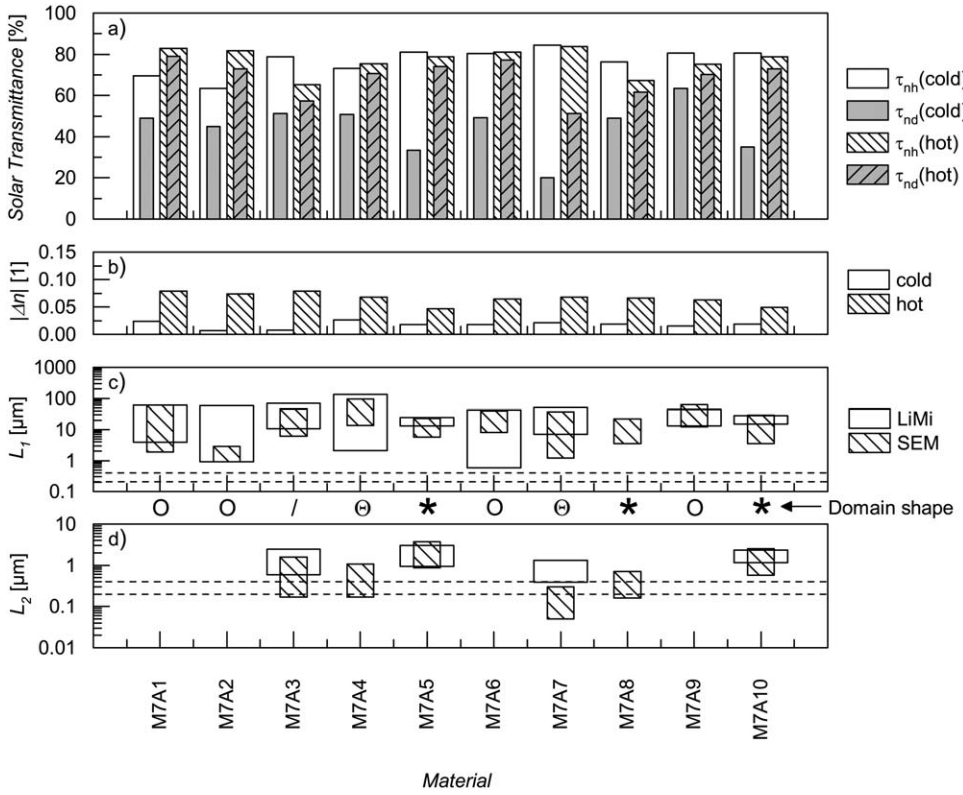

Figure 6. (a) Solar hemispheric (τ_{nh}; base color white) and solar diffuse transmittance (τ_{nd}; base color gray) of TSFD with UV-curable matrix material M7 below (no pattern) and above (hatching pattern) the threshold temperature (data from Part I[17]). (b) Refractive index difference of matrix and additive below (no pattern) and above (hatching pattern) the threshold temperature. Observed scattering domain shapes indicated with symbols ("O" spheres; "/" plates; "Θ" filament spheres; "*" dendrites) and their respective dimensions (c) L_1 (diameter) and (d) L_2 (if applicable, thickness of plates/filaments/dendrite branches) detected by optical light microscopy (LiMi; no pattern) and SEM (hatching pattern). Optimum scattering domain size range for spherical scattering domains is bounded by dashed lines.

Dendritic scattering domains with inappropriate diameter for light-shielding purposes were detected for TSFD M5A5, M5A8, and M5A10. Whereas thickness of dendrite branches of layers M5A5 and M5A10 was detected to be inadequate for efficient light scattering it was almost optimal for M5A8. Thus, TSFD M5A8, in contrast to layers M5A5 and M5A10, exhibited a highly significant reduction in solar hemispheric transmittance.[17] Solar diffuse transmittance of layers M5A5, M5A8, and M5A10 increased due to inappropriate diameter of dendrites.

Figure 5 represents parameters indicated above for TSFD with UV-curable matrix material M6. Observed domain shapes were spheres ("O"), plate-like domains ("/") and dendrites ("*"). TSFD M6A1 and M6A2 displayed spherical scattering domains with inappropriate size for optimum light-shielding efficiency and with vacuoles at their perimeter (interface matrix/additive). The achieved increase in solar hemispheric and diffuse transmittance was ascribed to the effect of the temporary vacuoles. Micrographs of layer M6A3 revealed plate-like domains with inappropriate diameter but almost optimal thickness for efficient back-scattering. Thus a significant reduction of solar hemispheric transmittance was ascertained upon heating. Solar diffuse transmittance of layer M6A3 remained almost constant upon exceeding the threshold temperature. However, the ratio of solar diffuse to solar hemispheric transmittance increased upon switching, which was attributed to the suboptimal scattering domain diameter.

Thickness of branches and diameter of dendrites observed for TSFD M6A10 were detected to be inappropriate for optimal back-scattering. Hence, merely a slight reduction of solar hemispheric transmittance was ascertained. The solar diffuse transmittance of layer M6A10 remained almost unchanged. Due to the increasing ratio of solar diffuse to solar hemispheric transmittance—similar to the observations for layer M6A3—again an increase in overall scattering efficiency and especially forward scattering was evident. This was attributed to the low thickness of dendrite branches and high diameter of dendrites, respectively.

Figure 6 represents parameters indicated above for TSFD with UV-curable matrix material M7. Observed domain shapes were spheres ("O"), plate-like domains ("/"), filament spheres ("Θ") and dendrites ("*"). Spherical scattering domains with inappropriate diameter for optimal light-shielding performance were detected for TSFD M7A1 and M7A2. Micrographs revealed vacuoles in these layers. Thus, these layers displayed an increase of solar hemispheric and diffuse transmittance upon heating due to the effect of the temporary vacuoles. Spherical scattering domains with inappropriate diameter were evident for layers

M7A6 and M7A9. TSFD M7A6 exhibited no vacuoles. Nevertheless, solar hemispheric transmittance change upon heating was insignificant.[17] According to the inappropriate scattering domain diameter, solar diffuse transmittance increased upon switching. Although scattering domain size was inappropriate for optimum back-scattering in TSFD M7A9, a slight decrease of solar hemispheric transmittance was detected upon heating. Accordingly, solar diffuse transmittance increased significantly.

Almost optimal thickness of plate-like domains for efficient overheating protection performance provided a reduction of solar hemispheric transmittance for layer M7A3 upon exceeding the threshold temperature. However, diameter of plates was inappropriate for efficient back-scattering. Thus, solar diffuse transmittance increased upon heating. Micrographs of TSFD M7A4 and M7A7 revealed spherical scattering domains built from filaments. The diameters of these domains were inappropriate for optimum light-shielding whereas the thickness of the filaments was almost optimal. However, between these filaments, voids were observed. Voids were assumed to act in the same manner as vacuoles. Thus, the increase of solar hemispheric transmittance of layer M7A4 was attributed to these voids (effect of the temporary vacuoles). Despite existence of voids, layer M7A7 showed a slight reduction in solar hemispheric transmittance. That might be attributed to a lower concentration of voids, thus yielding a mitigated effect on solar hemispheric transmittance. Both layers displayed an increase in solar diffuse transmittance due to the effect of the temporary vacuoles/voids as already described above. Dendritic scattering domains with inappropriate diameter for back-scattering were recorded for layers M7A5, M7A8, and M7A10. Thickness of branches of dendrites was detected to be appropriate for efficient light-shielding in layer M7A8 solely. Thus, out of these three TSFD, layer M7A8 displayed a significant reduction of solar hemispheric transmittance upon heating solely.[17] The increase in solar diffuse transmittance was attributed to the inappropriate scattering domain size.

For TSFD formulated with UV-curable resin matrix, these findings may lead to the conclusion that thermotropic additives exhibiting only little or almost no polar groups like paraffin waxes (A1, A2) or montan wax (A9) were not able to solubilize in the matrix resin upon melting due to the lack of interaction with the matrix (e.g., lack of hydrogen bonding). Consequently, the high interfacial tension established between matrix and additive forced the additive to form spheres to reduce overall interfacial forces. On the contrary, for more polar substances like fatty acids and fatty acid esters (with shorter nonpolar section compared to, e.g., paraffin waxes or montan wax) polar interaction forces were effectual to maintain solubilization of—at least significant fractions of—thermotropic additive upon melting of the additive. Upon cooling of the cast mixture of resin matrix and thermotropic additive prior to curing process, these thermotropic additives were forced to crystallize. Crystallization led to separation of additive from the resin matrix yielding two phase morphology. This transition from a solubilized/liquid to a nonsolubilized/solid state was effectual to establish nonspherical scattering domains. This was ascribed to the lack of viscous forces governing the additive droplet shape in the liquid state because there were no liquid additive droplets. In general, the spherical shape is usually in favor compared to other particle shapes due to its low surface/volume-ratio reducing interfacial forces compared to nonspherical shape of particles. Instead, crystallization of rather polar additives and thus domain form was governed by crystallographic alignment (predominant crystal form) of the thermotropic additives rather by viscous forces.

Summarizing, inappropriate scattering domain shape and/or size decreased solar hemispheric transmittance reduction upon heating and thus attenuated overheating protection performance of TSFD. This is according to scattering theory.[18,24] Defects (vacuoles, voids) resulting from processing yielded increasing solar hemispheric transmittance upon exceeding the threshold temperature (effect of temporary vacuoles). This is attributable to intense scattering at the boundary of matrix and scattering domain (matrix/vacuum interface), which is reduced upon melting of the additive.

CONCLUSION

Provided that refractive index data are appropriate, structure–property relationships established in "Establishment of Structure–Property Relationships" section yielded two major requirements for producing thermotropic systems with fixed domains (TSFD) with enhanced overheating protection performance:

1. Prevention of defects (vacuoles, voids)
2. Optimization of scattering domain shape and size by maintaining spherical scattering domains with diameters between 200 and 400 nm.

Vacuole formation in TSFD with thermoplastic matrix upon manufacturing was ascribed to different coefficient of thermal expansion (CTE) of matrix and additive combined with limited adhesion at the matrix/additive interface. Reducing the effect of thermal expansion by lowering processing temperature is not feasible due to processing reasons. Thus, vacuole formation in these TSFD might be prevented merely by adhesion promotion via covalent bonds between reactive moieties of matrix and additive.[19,25–28] TSFD M2A11 of this study is a prominent example for the potential of this approach.

In TSFD formulated with UV-curable resin matrix vacuole formation was ascribed to thermomechanical effects of different CTE of matrix and additive due to heat generation upon irradiation, crosslinking reaction and limited adhesion at the interface matrix/additive. In acrylate-based systems covalent bonds between matrix and additive cannot be achieved by introduction of epoxy or maleic-anhydride grafts. Hence, reduction of heat generation seems more feasible. Reduction of heat generation requires lowering absorbed energy by reducing the intensity and dose of UV-radiation. Investigations by Resch and coworkers[9,11] suggest viability of this approach. TSFD with similar UV-curable resin matrix and paraffin-type additive were produced by curing with low intensity UV-radiation. The samples lacked vacuoles and displayed a reduction of solar hemispheric transmittance upon exceeding the threshold temperature.[8,9,11,16]

Strategies for optimizing scattering domain size and shape can be deduced from scientific literature in related fields. Smaller

scattering domains might result from increasing number of crystallization nuclei (i.e., addition of nucleating agent) similar to achieved spherulite size reduction in polymers.[29,30] Heterogeneous nucleation in phase change materials is not only induced by "classical" nucleating agents but also by surfactants.[31–34] Surfactants might also change droplet size in emulsions of matrix materials and thermotropic additives during processing.[35] Nucleating agents and surfactants might also influence the shape of the scattering domains by changing matrix/additive interactions.

Another approach to maintain controlled size and shape of scattering domains is encapsulation of additives.[36,37] Simultaneously vacuole formation may be prevented when incorporating these capsules in a matrix material at temperatures close to ambient conditions. To the best of our knowledge Muehling et al.[12] were the first to apply this technique for TSFD formulation.

With respect to the optimization strategies regarding manufacturing process and TSFD formulation already pointed out, the optimization potential of TSFD formulated so far is considered to be high.

ACKNOWLEDGMENTS

This research project is funded by the State Government of Styria, Department Zukunftsfonds (Project number 5019). The efforts in determination of solar-optical properties of parts of the formulated TSFD by Astrid Rauschenbach (Polymer Competence Center Leoben GmbH, Leoben, AT (PCCL)), valuable input regarding scattering processes and scattering theory by Dieter P. Gruber (PCCL), support concerning UV equipment by Sandra Schlögl (PCCL) and compounding of materials with thermoplastic matrix by Karl Schnetzinger (APC Advanced Polymer Compounds, Gai, AT) are gratefully acknowledged. Furthermore, the authors wish to acknowledge the contributions of Arkema GmbH (Düsseldorf, DE), Baerlocher GmbH (Unterschleissheim, DE), Bayer Materials Science AG (Leverkusen, DE), Biesterfeld Interowa GmbH & Co. KG (Wien, AT), Brenntag CEE GmbH (Traun, AT), Chemson Polymer Additive AG (Arnoldstein, AT), Allnex Belgium SA/NV (formerly Cytec Surface Specialities Inc.; Drogenbos, BE), DuPont de Nemours (Deutschland) GmbH (Neu-Isenburg, DE), Evonik Degussa GmbH, High Performance Polymers (Marl, DE), Evonik Röhm GmbH (Darmstadt, DE), HDS-Chemie HandelsgesmbH (Wien, AT), Sasol Wax GmbH (Hamburg, DE) and Senoplast Klepsch GmbH (Piesendorf, AT).

REFERENCES

1. Yao, J.; Zhu, N. *Build. Environ.* **2012**, *49*, 283.
2. Wallner, G. M.; Resch, K.; Hausner, R. *Sol. Energy Mater. Sol. Cells* **2008**, *92*, 614.
3. Nitz, P.; Wagner, A. *BINE Themeninfo* **2002**, *I/02*, 1.
4. Nitz, P.; Hartwig, H. *Sol. Energy* **2005**, *79*, 573.
5. Seeboth, A.; Schneider, J.; Patzak, A. *Sol. Energy Mater. Sol. Cells* **2000**, *60*, 263.
6. Resch, K.; Wallner, G. M. In Proceedings of ISES Solar World Congress **2007**; Goswami, D. Y., Zhao, Y., Eds.; Springer: Berlin, **2007**, pp 541–545.
7. Resch, K.; Wallner, G. M. *Sol. Energy Mater. Sol. Cells* **2009**, *93*, 119.
8. Resch, K.; Wallner, G. M. *Polym. Adv. Technol.* **2009**, *20*, 1163.
9. Resch, K.; Wallner, G. M.; Hausner, R. *Sol. Energy* **2009**, *83*, 1689.
10. Resch, K.; Wallner, G. M.; Lang, R. W. *Macromol. Symp.* **2008**, *265*, 49.
11. Resch, K.; Weber, A. *Berg-Huettenmaenn. Monatsh.* **2011**, *156*, 429.
12. Muehling, O.; Seeboth, A.; Haeusler, T.; Ruhmann, R.; Potechius, E.; Vetter, R. *Sol. Energy Mater. Sol. Cells* **2009**, *93*, 1510.
13. Bühler, F. S.; Hewel, M. German Pat. DE 19,841,234 C1 (**1998**).
14. DeArmitt, C.; Mc Kee, G. E. Eur. Pat. EP 1,985,663 A1 (**2008**).
15. Weber, A.; Resch, K. In Conference Proceedings of the 6th ENERGY FORUM; Economic Forum, Ed.: Munich, **2011**; p 73.
16. Weber, A.; Resch, K. *J. Polym. Res.* **2012**, *19*, 1.
17. Weber, A.; Resch, K. *J. Appl. Polym. Sci.*, accepted manuscript.
18. Nitz, P. Optical modelling and characterisation of thermotropic systems. Dissertation: Freiburg I.B., **1999**.
19. Baur, E.; Brinkmann, S.; Osswald, T. A.; Schmachtenberg, E. Saechtling-Kunststoff-Taschenbuch; Hanser: München, **2007**.
20. Schimmelpfennig, M.; Weber, K.; Kalb, F.; Feller, K.-H.; Butz, T.; Matthäi, M. In Jahrbuch für den Praktiker; Ziolkowsky, B., Ed.; Verlag für chemische Industrie: Augsburg, **2007**; Vol. *50*, pp 417–429.
21. Su, J.-F.; Wang, X.-Y.; Wang, S.-B.; Zhao, Y.-H.; Zhu, K.-Y.; Yuan, X.-Y. *Polym. Compos.* **2011**, *32*, 810.
22. Wang, X.-Y.; Su, J.-F.; Wang, S.-B.; Zhao, Y.-H. *Polym. Compos.* **2011**, *32*, 1439.
23. Derkach, S. R. *Adv. Colloid Interface Sci.* **2009**, *151*, 1.
24. Nitz, P.; Ferber, J.; Stangl, R.; Wilson, H. R.; Wittwer, V. *Sol. Energy Mater. Sol. Cells* **1998**, *54*, 297.
25. Koning, C.; van Duin, M.; Pagnoulle, C.; Jerome, R. *Prog. Polym. Sci.* **1998**, *23*, 707.
26. Kayano, Y.; Keskkula, H.; Paul, D. *Polymer* **1997**, *38*, 1885.
27. Luyt, A.; Krupa, I.; Assumption, H.; Ahmad, E.; Mofokeng, *J. Polym. Test.* **2010**, *29*, 100.
28. Novák, I.; Krupa, I.; Luyt, A. S. *J. Appl. Polym. Sci.* **2005**, *95*, 1164.
29. Ehrenstein, G. W.; Riedel, G.; Trawiel, P. Praxis der thermischen Analyse von Kunststoffen; Hanser: München, **2003**.

30. Fairgrieve, S. *Rapra Rev. Rep.* **2005**, *16*, 187.
31. Smith, K. W.; Bhaggan, K.; Talbot, G.; van Malssen, K. F. *J. Am. Oil Chem. Soc.* **2011**, *88*, 1085.
32. Zhang, X.-X.; Fan, Y.-F.; Tao, X.-M.; Yick, K.-L. *J. Colloid Interface Sci.* **2005**, *281*, 299.
33. Günther, E.; Huang, L.; Mehling, H.; Dötsch, C. *Thermochim. Acta* **2011**, *522*, 199.
34. Chari, K.; Antalek, B.; Kowalczyk, J.; Eachus, R. S.; Chen, T. *J. Phys. Chem. B* **1999**, *103*, 9867.
35. Tadros, T. F. In Emulsion Science and Technology; Tadros, T. F., Ed.; Wiley-VCH: Weinheim, **2009**; pp 1–56.
36. Zhao, C.; Zhang, G. *Renewable Sustainable Energy Rev.* **2011**, *15*, 3813.
37. Landfester, K. *Angew. Chem.* **2009**, *121*, 4556.